Magnetothermal oscillations in RuO_2, OsO_2, and IrO_2

J. E. Graebner and E. S. Greiner*
Bell Laboratories, Murray Hill, New Jersey 07974

W. D. Ryden
Bell Laboratories, Allentown, Pennsylvania 18104

(Received 29 October 1975)

Magnetothermal oscillations in RuO_2, OsO_2, and IrO_2 at 1.3 K and fields up to 10.5 T allow a detailed mapping of the Fermi surfaces of these isomorphous transition-metal oxides. Relatively simple Fermi surfaces are deduced for RuO_2 and OsO_2, though magnetic breakdown of orbits in the former give rise to uncertainties in the interpretation of the data. A very complicated Fermi surface is found to fit the data of IrO_2. The topology of the Fermi surfaces in all three cases was suggested by perliminary band-structure calculations of Mattheiss. The same band structure was used for all three materials, with slight modifications between isoelectronic RuO_2 and OsO_2 to account for greater spin-orbit coupling in OsO_2. The fact that the same band structure can be made to fit the (extra-electron) IrO_2 at a higher Fermi energy confirms the basic correctness of the band structure over an energy range of ~ 0.5 eV.

I. INTRODUCTION

Transition-metal oxides of the rutile and related structures display a variety of interesting electrical properties. Among the most notable are the metal-insulator transitions of the vanadium oxides. The high transition temperatures, however, preclude investigation of the metallic state by means of typical low-temperature Fermi-surface (FS) techniques. Reliance must be made on nontransforming materials of similar structure. We present FS measurements in rutile-structure RuO_2, OsO_2, and IrO_2, all of which remain good metals down to liquid-helium temperatures. In addition to their potential contribution to the study of metal-insulator transitions, these three materials provide a somewhat unique series of metals with nearly identical lattice parameters (within $\sim 1\%$) but different electronic character. One would expect isoelectronic RuO_2 and OsO_2 to differ principally in spin-orbit coupling, and OsO_2 and IrO_2 to differ simply in Fermi level, due to the extra electron of Ir. Thus one can examine a band structure experimentally over a range of ~ 0.5 eV, which is in contrast to the usual limitation of FS measurements to within a few meV of the Fermi level. Mattheiss has performed combined tight-binding–APW (augmented plane wave) band calculations for the rutile structure. The tetragonal structure and its Brillouin zone are shown in Fig. 1. The lattice parameters used here[1] are given in Table I. Figure 2 shows preliminary results of the t_{2g} portion of the band-structure calculations by Mattheiss,[2] along with our empirical modifications (see below). The estimated Fermi levels are indicated for the three materials. We note that the separation of the fourth and fifth bands along ΓZ is proportional to the spin-orbit coupling.[2]

Preliminary reports of the present work[3] and related magnetoresistance measurements on[4] IrO_2 have been made. De Haas–van Alphen effect[5] and magnetoresistance[6,7] data for RuO_2 were obtained by Marcus. Slivka and Langenberg[8] have reported cyclotron resonance data in RuO_2.

II. EXPERIMENTAL PROCEDURE

Single crystal samples were grown by the oxygen-transport technique[9] with residual resistance ratios RRR $[=r(300\text{ K})/r(4.2\text{ K})]$ of 20000, 150, and 1400 for RuO_2, OsO_2, and IrO_2, respectively. Measurements were also made on samples of RuO_2 and OsO_2 with similar RRR's, grown by the same technique and generously provided by Marcus. There was no observable dependence of the data on the sample source.

The samples were mounted on a graphite post in a device[10] allowing 360° rotation in a plane containing the magnetic field vector $\vec{H}$. Magnetic fields to 10.5 T were provided by a superconducting solenoid. The field strength was monitored by a copper magnetoresistance probe.[11] A car-

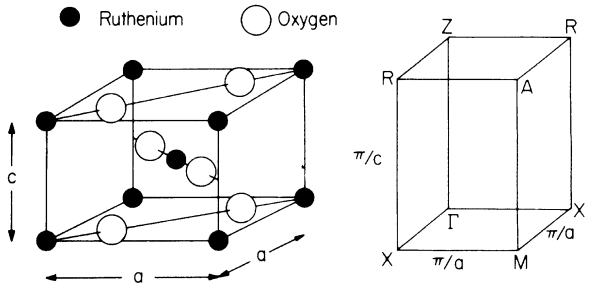

FIG. 1. Crystal structure and $\frac{1}{8}$ of Brillouin zone for RuO_2. Lattice parameters for OSO_2 and IrO_2 differ from RuO_2 by less than $\sim 1\%$.

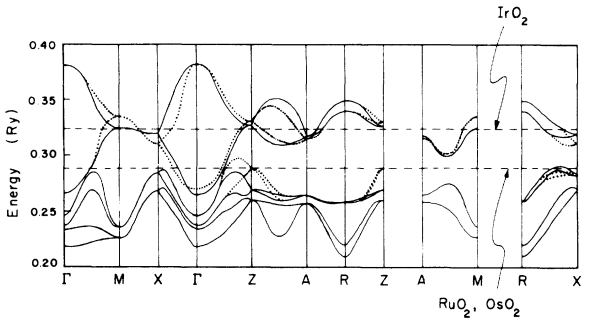

FIG. 2. Solid lines: Preliminary APW band structure for the rutile structure. Dashed lines give the estimate Fermi energies for RuO_2, OsO_2, and IrO_2. Dotted lines: empirical modifications of band structure to account for the Fermi surface proposed here.

bon resistance thermometer was mounted on the sample to monitor the Landau quantum oscillations of temperature as a function of field strength. The data were all taken at an average temperature of ~1.3 K, with a modulation field of ~11 Hz provided by a NbZr solenoid inside the main field windings. The data were digitized and recorded on magnetic tape, then analyzed by computer calculation of the Fourier transform of each sweep up or down in field strength.[12] The spectra at different angles of orientation of $\vec{H}$ with respect to crystal axes then show how the frequencies[13] (extremal cross sections of FS perpendicular to $\vec{H}$) vary with field direction.

TABLE I. Lattice parameters (Å).

	a	c
RuO_2	4.4919	3.1066
OsO_2	4.5003	3.1839
IrO_2	4.4983	3.1544

III. RESULTS

A. RuO_2

The data for $\vec{H}$ lying in the {100}, {110}, and {001} planes of RuO_2 are shown in Fig. 3. Two nonsymmetry planes were also investigated in detail but are not shown here. Frequencies α and β seem to merge in an upward cusp for all directions except those approaching the c axis. α has an overall minimum at 35° from ⟨110⟩ in a (110) plane. Frequencies γ and δ in the {001} plane seem to differ by a constant amount until they disappear. In a (100) plane γ appears to split into two branches in a nonsimple manner (see below) while δ is not readily observable. Frequency ϵ is a smooth function of angle for all field directions.

Figure 4 shows α and β in {110} and γ in {100} on an expanded scale. γ is seen to consist of two separate branches, the upper coming in to ⟨a⟩ with zero slope, the lower rising rapidly but disappearing before it reaches ⟨a⟩. α and β are seen to vary

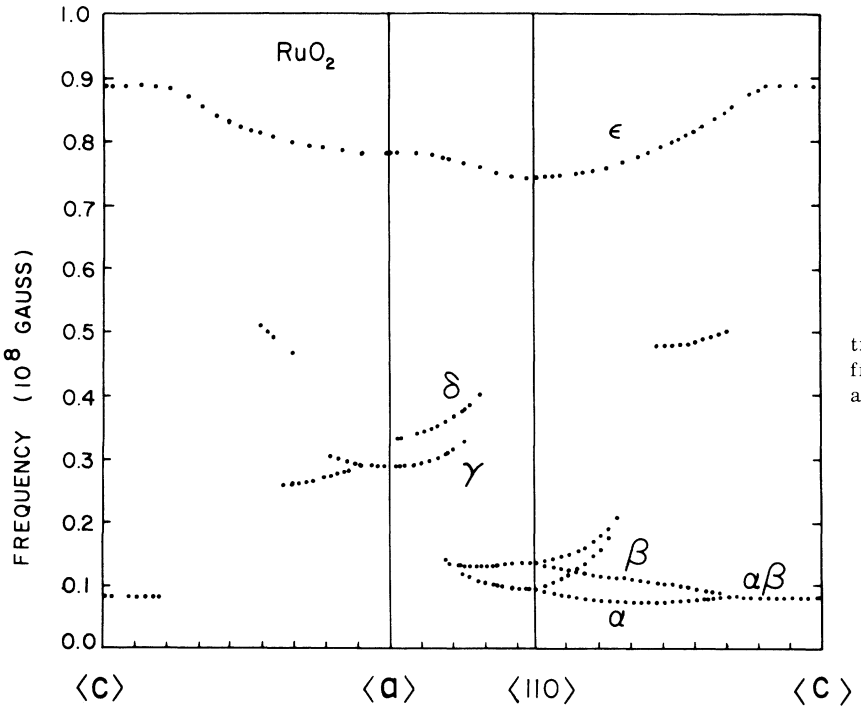

FIG. 3. Magnetothermal oscillation frequencies in RuO_2 vs magnetic field direction with respect to crystal axes for three principal planes.

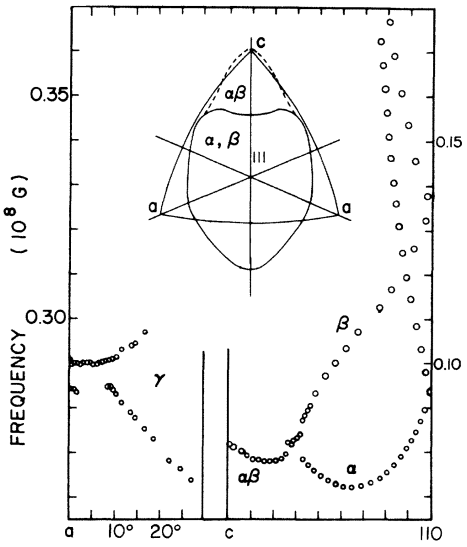

FIG. 4. Expanded view of RuO_2 frequencies γ, α, β, and $\alpha\beta$ in the {100} and {110} planes. The inset shows a stereographic projection about ⟨111⟩ of directions where α and β are seen separately and where $\alpha\beta$ is seen.

smoothly but to either disappear or change abruptly, at 65° from ⟨110⟩, to the branch labeled $\alpha\beta$ This behavior is seen only for directions approaching the c axis, as is shown in the stereogram in Fig. 4. It is not clear precisely how the α and β branches are connected to the $\alpha\beta$ branch, if indeed they are connected at all.

B. OsO_2

The data for OsO_2, Fig. 5, consist of two branches, α and β, which are separate and single-valued over all three principal planes investigated.

C. IrO_2

The data for the three principal planes of IrO_2, Fig. 6, are much more complicated than in RuO_2

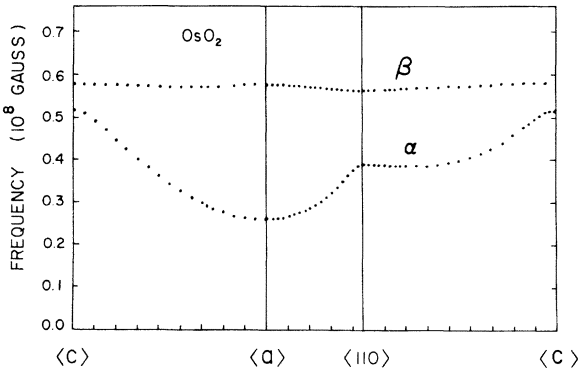

FIG. 5. Magnetothermal oscillation frequencies in OsO_2 vs magnetic field direction with respect to crystal axes for three principal planes.

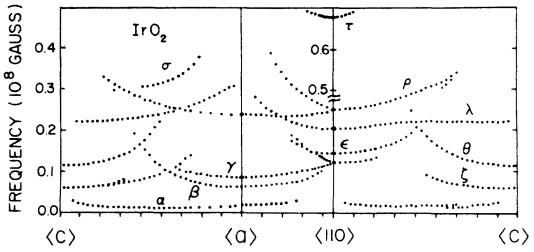

FIG. 6. Magnetothermal oscillation frequencies in IrO_2 vs magnetic field direction with respect to crystal axes for three principal planes. Note that the frequency τ has been shifted down in frequency.

or OsO_2. As many as eight frequencies are seen at any given angle, not counting the many second harmonics not shown. Three low-symmetry planes were also investigated in detail but are not shown in Fig. 6. It was clear from the low-symmetry planes that the (100) plane and ~2° to either side of it comprise a region of small or zero amplitude for frequency λ. Otherwise, λ seems to be a simple, single-valued function of angle.

Frequency α shows an over-all minimum at

TABLE II. Frequencies at high-symmetry directions.

	Label	$\hat{H}$	Frequency (10^8 G)
RuO_2	α_{min}	35° from {110}, [110] plane	0.0719
	β	35° from {110}, [110] plane	0.105
	α	{110}	0.0930
	β	{110}	0.1360
	$\alpha\beta$	⟨c⟩	0.082
	γ	⟨a⟩	0.287
	δ	⟨a⟩	0.335
	ϵ	⟨a⟩	0.783
	ϵ	⟨c⟩	0.889
	ϵ	{110}	0.742
OsO_2	α	⟨a⟩	0.260
	α	⟨c⟩	0.516
	α	{110}	0.387
	β	⟨a⟩	0.577
	β	⟨c⟩	0.577
	β	{110}	0.563
IrO_2	α_{min}	52° from ⟨c⟩ toward ⟨a⟩	0.0125
	β	⟨a⟩	0.0625
	ζ	⟨c⟩	0.060
	γ	⟨a⟩	0.088
	γ	{110}	0.122
	ϵ	{110}	0.143
	λ	⟨a⟩	0.32
	λ	⟨c⟩	0.222
	λ	{110}	0.204
	ρ	⟨a⟩	0.238
	ρ	{110}	0.251
	τ	{110}	0.682
	θ	⟨c⟩	0.115

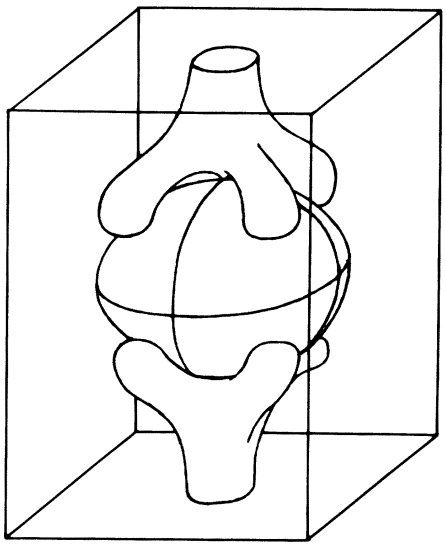

FIG. 7. Three-dimensional view of the proposed Fermi surface for RuO_2.

52° away from ⟨c⟩ toward ⟨a⟩ and seems to be single valued for all directions.

The extremal frequencies at high-symmetry directions for all three oxides are collected in Table II.

IV. DISCUSSION

A. RuO_2

We see from the partial band structure of Fig. 2 that a closed, Γ-centered electron surface is predicted for RuO_2 and OsO_2. We will see that the data for RuO_2 and OsO_2 are both fit better if the third and fourth t_{2g} bands are moved up to the Fermi level at Z, as shown by the dotted curves.

For RuO_2, we identify frequency ϵ with the Γ-centered electron piece. The surface at Γ in Figs. 7–9 is the result of a simple geometrical model fitted to the data and is probably accurate in radius to a few percent. To explain the remaining data for RuO_2, we adjust the t_{2g} bands at Z to intersect just *above* the Fermi level, forming a small fourth-zone hole pocket centered at Z, just within the fifth-zone hole surface. We further postulate that the latter surface bulges out into knobby arms pointing roughly from Z toward M. The enlarged ends on the arms give rise to minimum and maximum areas for most field orientations, corresponding to α and β, respectively. The exact angular dependence of the cross-sectional extremal areas is of course difficult to calculate on surfaces of such low symmetry, but several features are clearly seen to correspond to peculiarities of the data. The overall minimum for α occurs at 55° from ⟨c⟩ in the {110} plane, but at this angle β is *not* at a relative maximum area as a function of angle. Furthermore, the angles at which α and β merge and disappear in the data correspond well to those angles at which the model ceases to support extremal orbits: at 28° from ⟨110⟩ in the {001} plane and 117° and 34° from ⟨c⟩ in the {110} plane. Furthermore, the first two instances are upward cusps while for the last (34°) the higher frequency β is *decreasing* as it approaches α. Such behavior might be expected from the model in Fig. 8 owing to the unusual shape of the end of the arm. The only failing of the model is that it does not give rise to an orbit corresponding to $\alpha\beta$, nor does it predict a sudden disappearance of α or β just prior to their merging. Perhaps there is some feature we have not taken into account, such as an accidental degeneracy between the arm and the Γ-centered electron surface which somehow provides a cutoff point.

If one assumes that the small hole ellipsoid and the waist of the larger hole surface, both centered at Z, are connected by partial magnetic

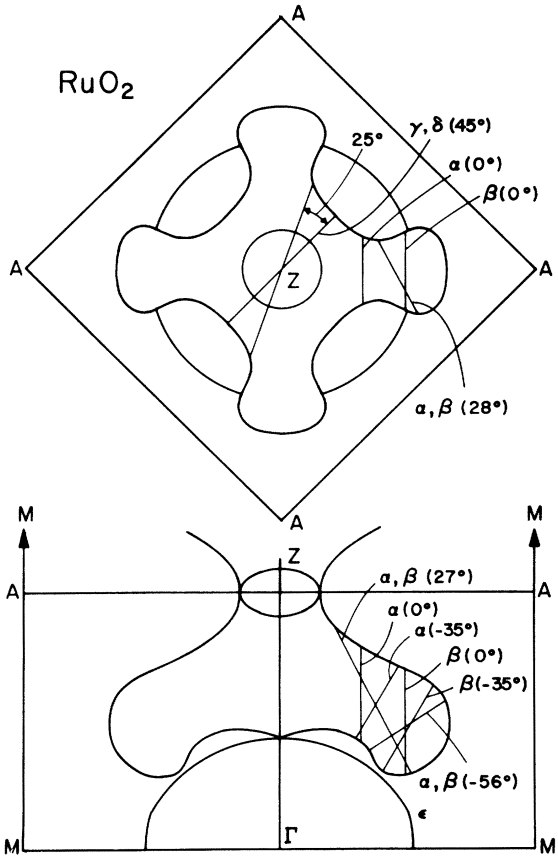

FIG. 8. (110) section and c-axis view of the Fermi surface proposed for RuO_2. Various orbits are shown for α, β, and γ. The angles given in parentheses are angles between the magnetic field and the ⟨110⟩ axis.

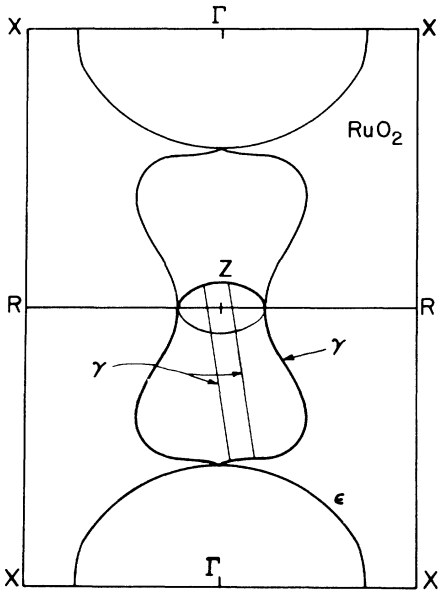

FIG. 9. (100) section of the Fermi surface proposed for RuO_2. The heavy outline shows the orbit proposed to explain the data labeled γ in Figs. 3 and 4 for $\vec{H} \parallel \langle a \rangle$. The two slanted lines show the planes of the orbits labeled γ when $\vec{H}$ is rotated from $\langle a \rangle$ toward $\langle c \rangle$ (see text).

breakdown in the *ZAR* plane, one can explain frequencies γ and δ. The size of the hole ellipsoid has been chosen equal to the difference $f_\delta - f_\gamma = 0.048 \times 10^8$ G. For $\vec{H} \parallel \langle a \rangle$, Fig. 9, we interpret γ as shown by the heavy outline around the bottom half of the hour-glass-like cross section and breaking down across the waist to traverse the top half of the hole pocket, then returning to the bottom half of the hour glass. We interpret δ as the same orbit but with the proper combination

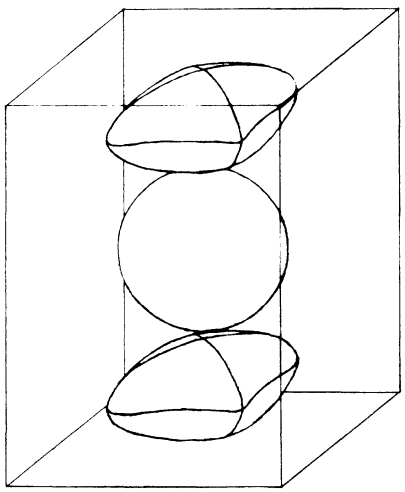

FIG. 10. Three-dimensional view of the Fermi surface proposed for OsO_2.

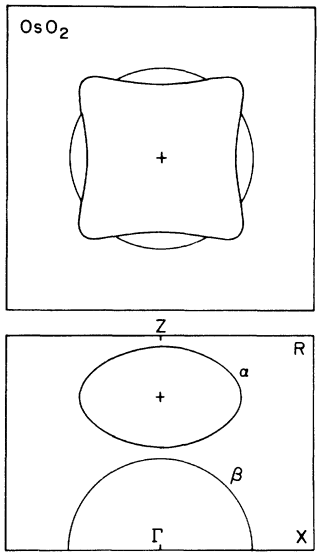

FIG. 11. (100) section and c-axis view of the Fermi surface proposed for OsO_2.

of gap breakdowns and nonbreakdowns that one and a half circuits of the ellipsoid are made before returning to the hour-glass orbit. Since the orbits are both holelike, the frequencies should add, i.e., $f_\delta = f_\gamma + f_{\text{ellipsoid}}$ as observed. The model is also consistent with both γ and δ increasing rapidly in the $\{001\}$ plane with a nearly constant difference between them and disappearing $\sim 25°$ from $\langle 100 \rangle$ as the orbits open out discontinuously onto the arms (Fig. 8). Rotating $\vec{H}$ from $\langle a \rangle$ up toward $\langle c \rangle$ should result in γ splitting into several orbits like those shown in Fig. 9, one of which is locked near the dimple at the bottom of the hour glass and decreases with angle, the other of which increases with angle as it approaches the bases of the arms. A connection along ΓZ with the electron surface is suggested by magnetoresistance experiments[7] which indicate open orbits along the c axis. Any more detailed interpretation of γ and δ must await a very detailed interpretation of the frequency branches in the vicinity of $\langle a \rangle$.

We have no interpretation for the short branches of data at $\sim 0.5 \times 10^8$ G in the $\{100\}$ and $\{110\}$ planes.

B. OsO_2

The interpretation of the OsO_2 data is far simpler than for RuO_2. The larger frequency β we associate with the Γ-centered electron sheet which now is $\sim 20\%$ smaller in radius than in RuO_2 and spherical to within 1% in radius.

The smaller frequency α is attributed to a closed, fifth-band hole surface located along ΓZ. The absence of any other observable orbits indi-

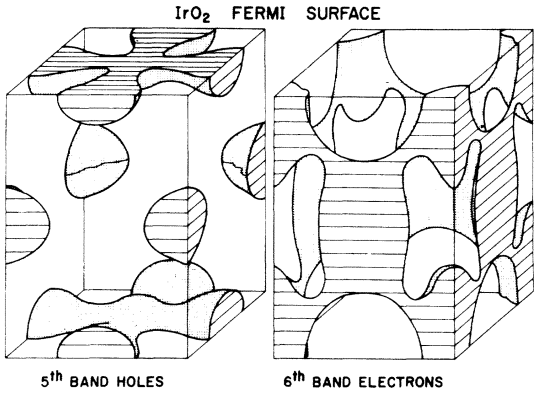

FIG. 12. Three-dimensional view of the Fermi surface proposed for IrO_2. Errors in drafting have accidentally eliminated the ⟨101⟩-directed open orbits along the zone face diagonal (see Fig. 13).

cated that the upper two t_{2g} bands at Z fall *below* E_F, not above E_F as in RuO_2. The simple pillow-like surface shown in Figs. 10 and 11 fits the data well but has higher symmetry than required by the site. For instance, the four corners could possibly droop down toward the ΓXM plane to resemble even more closely the corresponding surface in RuO_2. The fact that no connection along ΓZ between the two surfaces is indicated by the data is consistent with greater spin-orbit splitting of the bands along ΓZ.

C. IrO_2

A model of the FS of IrO_2 was obtained by adjusting the t_{2g} bands in Fig. 2 until a FS was obtained which supported orbits that could be identified with the data of Fig. 6. The result of this procedure is shown in Figs. 12 and 13. We have included a bridge in the XA direction to account for frequency α. Frequency λ is due to a simple piece and is identified with the closed surface at M. The data were inverted[14] in an unambiguous way, owing to the center of symmetry at M, to obtain the principal cross sections shown at M in Fig. 13. The absence of λ data in the (100) planes indicates a small area of contact between the X- and M-centered sheets along XM. The orbit centered at X is identified with frequency ζ and the radius ζ_{XM} is just the difference between length XM and λ_{XM}, or 0.363 Å^{-1}. (ζ_{XM} indicates the radius, in the XM direction, of the principal cross section of ζ.) Using an ellipse as an approximation of the area of orbit ζ in the basal plane, we obtain $\zeta_{\Gamma X} = 0.051$ Å$^{-1} = \gamma_{\Gamma X}$. We note that the model is consistent with two nearly identical branches for ζ as the field is rotated away from ⟨a⟩ in a {100} plane, as observed. From the angular dependence of ζ and γ and the assumption of a bridge toward A, we estimate $\gamma_{XR} = 0.40$ Å^{-1} with the cross-sectional shape indicated. With the assignment of τ and θ to orbits centered

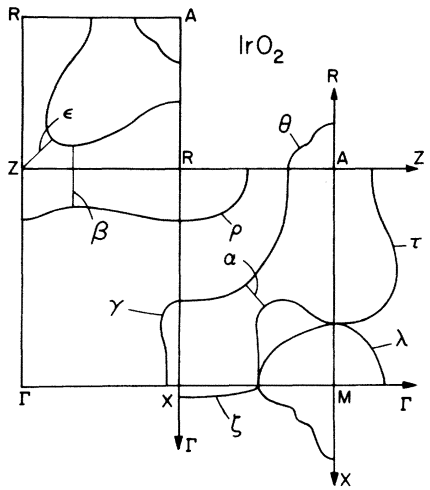

FIG. 13. Sections of the Fermi surface proposed for IrO_2. Lower-case Greek letters indicate orbits assigned to the various data of Fig. 6.

TABLE III. Radii for the cross sections at high-symmetry directions.

	Radius label	Length (Å^{-1})
RuO_2	$\alpha_{\sim\Gamma A}$	0.33
	$\alpha_{\Gamma M}$	0.12
	$\beta_{\sim\Gamma A}$	0.39
	$\beta_{\Gamma M}$	0.15
	Z-centered ellipsoid$_{ZR}$	0.155
	Z-centered ellipsoid$_{Z\Gamma}$	0.095
	$\epsilon_{\Gamma M}$, $\epsilon_{\Gamma X}$	0.520
	$\epsilon_{\Gamma Z}$	0.445
OsO_2	$\alpha_{\Gamma Z}$	0.234
	$\alpha_{\Gamma X}$	0.337
	$\alpha_{\Gamma M}$	0.500
	$\beta_{\Gamma Z}$, $\beta_{\Gamma X}$, $\beta_{\Gamma M}$	0.417
IrO_2	$\alpha_{\sim MR}$	0.062
	β_{ZR}	0.11
	$\beta_{Z\Gamma}$	0.1725
	γ_{XR}	0.40
	$\gamma_{X\Gamma}$	0.051
	$\zeta_{X\Gamma}$	0.051
	ζ_{XM}	0.363
	ϵ_{ZA}	0.19
	$\epsilon_{Z\Gamma}$	0.228
	θ_{AR}	0.21
	θ_{AZ}	0.17
	λ_{MX}	0.335
	λ_{MA}	0.288
	$\lambda_{M\Gamma}$	0.232
	τ_{AM}	0.708
	τ_{AZ}	0.17
	ρ_{RA}	0.31
	ρ_{RX}	0.235

at A and taking into account their angular dependence, we obtain the shapes shown around A. Because of the low symmetry of the bridge, the shape of the cross section at minimum α cannot even be estimated from the present measurements and thus it is assumed to be circular in the figures.

The fifth band hole surface in the shape of a cross is proposed to account for frequencies ϵ, β, and ρ. The angular range of ρ in the $\{001\}$ plane indicates a neck dimension $\beta_{ZR} \approx 0.11$ Å^{-1} and in the $\{110\}$ plane indicates $\epsilon_{Z\Gamma} \approx 0.228$ Å^{-1}. $\beta_{\min}$ and $\epsilon_{\min}$ then determine ϵ_{ZA} and $\beta_{Z\Gamma}$, assuming elliptical cross sections. The angular dependence of ρ indicates a shape about R as drawn. The assignments of ϵ, β, and ρ are particularly convincing when one notices the presence of an extra branch joining ρ from below just as it disappears in the $\{100\}$ and $\{110\}$ planes. The model predicts that β should join ρ in just this manner.

No interpretation is given for the short frequency branch observed over ~30° in the $\{100\}$ plane at $(0.3-0.4)\times10^8$ G.

D. General

The radii for the cross sections at high-symmetry directions are collected in Table III. The Fermi surfaces proposed here are in general agreement with previous data reported briefly for[5] RuO_2 with the exception of F_3 of Ref. 5. The precision of measurement is not sufficient to assign it to an orbit on our model, and over much of its range it may, in fact, be a harmonic of F_2.

Our model proposed for the FS of IrO_2 is in good agreement with the detailed magnetoresistance measurements of Ryden *et al.*[4] requiring open orbits along $\langle a\rangle$, $\langle c\rangle$, and the zone face diagonal XA. The model for RuO_2 is in agreement with magnetoresistance data of Ryden *et al.*[7] which require open orbits along $\langle c\rangle$, but in disagreement with the magnetoresistance data of Marcus.[6] However, the work of Ryden *et al.* indicates that the axes in Ref. 6 are mislabeled.

V. CONCLUSIONS

The detailed magnetothermal oscillations presented here have been compared with Fermi-surface models deduced from a modified band-structure calculation of Mattheiss. Reasonably good agreement is obtained for RuO_2 but with some ambiguities remaining, due perhaps to magnetic breakdown of certain orbits. Excellent fits are obtained for both OsO_2 and IrO_2 with a simple Fermi surface for the former and a very complicated one for the latter. The differences between the band structures for RuO_2 and OsO_2 are small. The effect of greater spin-orbit splitting along ΓZ in OsO_2 is observed. The Fermi energy for IrO_2 lies ~0.5 eV above that for RuO_2 and OsO_2. Thus, the face that the band structure gives a good description of the data for all three oxides confirms the basic correctness of the calculation.

ACKNOWLEDGMENTS

We thank L. M. Mattheiss for many fruitful conversations and S. M. Marcus for the use of his RuO_2 and OsO_2 samples.

---

*Now retired.

[1]C. E. Bowman, Acta Chem. Scand. 24, 116 (1970).
[2]L. F. Mattheiss (unpublished).
[3]J. E. Graebner and W. D. Ryden, Bull. Am. Phys. Soc. 15, 312 (1970).
[4]W. D. Ryden, W. A. Reed, and E. S. Greiner, Phys. Rev. B 6, 2089 (1972).
[5]S. M. Marcus and S. R. Butler, Phys. Lett. A 26, 518 (1968).
[6]S. M. Marcus, Phys. Lett. A 28, 191 (1968).
[7]Also, W. D. Ryden (unpublished).
[8]R. T. Slivka and D. N. Langenberg, Phys. Lett. A 28, 169 (1968).
[9]D. B. Rogers, R. D. Shannon, A. W. Sleight, and J. L. Gillson, J. Inorg. Chem. 8, 841 (1969).
[10]M. H. Halloran and J. E. Kunzler, Rev. Sci. Instrum. 39, 1501 (1968).
[11]M. H. Halloran, J. H. Condon, J. E. Graebner, J. E. Kunzler, and F. S. L. Hsu, Phys. Rev. B 1, 366 (1970).
[12]J. E. Graebner and J. A. Marcus, Phys. Rev. 175, 659 (1968).
[13]Frequency in units of 10^8 G = 1.048× (area in units of Å^{-2}).
[14]We thank L. F. Mattheiss for the use of his program incorporating the inversion scheme of F. M. Mueller, Phys. Rev. 148, 636 (1966).

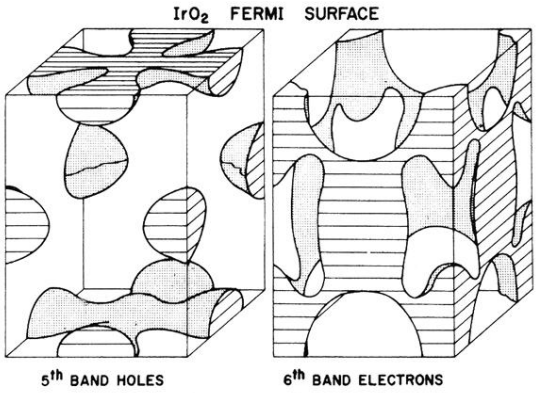

FIG. 12. Three-dimensional view of the Fermi surface proposed for IrO_2. Errors in drafting have accidentally eliminated the ⟨101⟩-directed open orbits along the zone face diagonal (see Fig. 13).